RSC Advances

PAPER

View Article Online
View Journal | View Issue

Cite this: *RSC Adv.*, 2020, **10**, 20302

Fabrication of low-fouling, high-loading polymeric surfaces through pH-controlled RAFT†

Alexander H. Jesmer,[a] Vincent Huynh[a] and Ryan G. Wylie *[ab]

Received 23rd March 2020
Accepted 18th May 2020

DOI: 10.1039/d0ra02693j

rsc.li/rsc-advances

Low-fouling and high-loading surfaces are increasingly important for biosensing and blood purification technologies. Selective and efficient target binding from complex media can be achieved with poly(carboxybetaine) (pCB) surfaces that consist of a dense brush layer to resist non-specific protein adsorption and a sparse "mushroom" upper layer for high-density capture agent immobilization (*i.e.* high-loading). We developed pH-controlled surface-reversible addition–fragmentation chain-transfer (S-RAFT) polymerization to simplify fabrication of multi-modal, low-fouling and high-loading pCB surfaces without the need for quenching or re-initiation steps, toxic transition metals or light irradiation. Multi-modal polymer layers were produced through partial polymer termination by temporarily raising the pH to aminolyse a fraction of dormant chain transfer agents (CTAs); remaining polymer chains with intact CTAs continued uninterrupted extension to create the "mushroom" upper layer. The multi-modal pCB surfaces were low-fouling towards proteins (<6.7 ng cm^{-2}), and macrophages. Compared to mono-modal brush surfaces, multi-modal pCB surfaces were high-loading with 5-fold greater capture agent immobilization (*e.g.* antibody) and 4-fold greater target binding (*e.g.* biotin-fluorescein).

1. Introduction

Bioactive polymeric surface coatings for low-fouling bio-interfaces are being developed for biomolecule sensing in complex fluids and blood purification.[1–6] To date, a variety of polymeric materials have been used to achieve low-fouling surfaces such as poly(ethylene glycol) (PEG),[7] fluorinated polymers,[8] and zwitterionic polymers.[5] Poly(carboxybetaine) (pCB) has been identified as a zwitterionic polymer that both resists non-specific protein adsorption and is readily functionalized with biomolecules that act as capture agents for target molecule binding. Capture agents can be anchored to pCB's carboxylic acid groups while maintaining low-fouling properties towards proteins.[9] Furthermore, enzymes and antibodies conjugated to pCB maintain or increase in activity[10] and thermostability by restricting conformational transitions,[11] making it optimal for bioactive low-fouling surfaces.

Polymer surface coatings are produced by one of two methodologies: (1) "graft-to", where the end group of pre-synthesized polymer are covalently bonded to a surface; or (2) "graft-from", where polymerization is initiated from the surface.[12] Graft-to polymer densities are limited by the polymer chain's radius of gyration (R_g) leading to low density "pancake" or "mushroom" polymer conformations.[13] Graft-from yields polymer densities that exceed the R_g imposed limit, and extends polymer chains in a brush configuration.[13] While graft-from's high polymer density improves fouling resistance,[14] biomolecule immobilization is limited to a monolayer on the brush surface; polymer side-chains are inaccessible due to tight polymer packing.[15] In contrast, graft-to's lower polymer density yields surfaces with greater loading potential but also increases fouling due to lower polymer surface coverage.

Bimodal architectures demonstrate high surface loading while remaining low-fouling,[9,15,16] combining the advantages of graft-from and graft-to. Bimodal polymer surfaces consist of a short dense polymer layer that resists protein fouling, and a sparse layer for greater biomolecule immobilization. Bimodal architectures have been synthesized previously *via* surface initiated-atom transfer radical polymerization (SI-ATRP) and surface initiated-photoiniferter mediated polymerization (SI-PIMP)[9,15,16] *via* two-step procedures that require termination and radical re-initiation steps, copper or surface exposure to light. The methods require two independent sequential radical polymerizations, where the first polymerization is fully quenched before re-initiation of the synthesis of the second polymer layer.

To decrease synthetic complexity and expand accessibility, we developed pH-controlled S-RAFT for multimodal polymer architectures that avoids radical quenching, re-initiation and multiple CTA-immobilization steps (Fig. 1). The procedure terminates a subpopulation of CTAs during polymerization to establish the dense polymer layer, while the remaining chains

[a]*Department of Chemistry and Chemical Biology, McMaster University, Hamilton, Ontario, L8S 4M1, Canada. E-mail: wylier@mcmaster.ca*

[b]*School of Biomedical Engineering, McMaster University, Hamilton, Ontario, L8S 4M1, Canada*

† Electronic supplementary information (ESI) available. See DOI: 10.1039/d0ra02693j

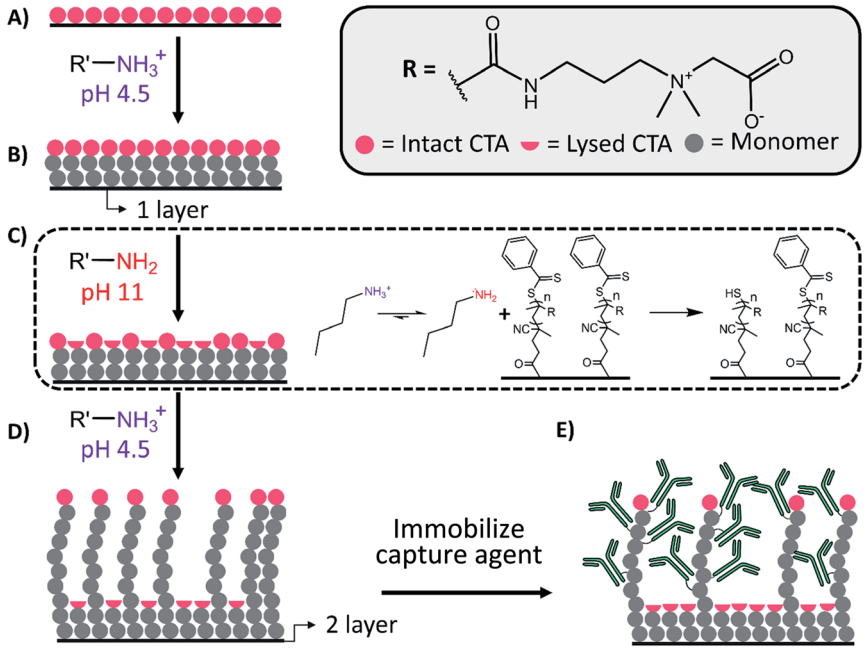

Fig. 1 Schematic for the synthesis of bimodal pCB layers *via* pH-controlled S-RAFT for enhanced capture agent immobilization on low-fouling surfaces. (A) Surface functionalized with a monolayer of RAFT CTA. (B) Synthesis of the dense pCB layer at pH 4.5 in the presence of a protonated primary amine, butylamine (pK_a of 10.5). (C) Temporary increase in pH (4.5 to 11) to deprotonate butylamine for the partial aminolysis of immobilized CTA. (D) pH returned to 4.5 for continued polymerization to yield the lower density, high loading pCB layer; pH 4.5 re-protonates butylamine to prevent further CTA aminolysis. (E) Compared to monomodal architectures, bimodal pCB architectures yield greater surface densities of accessible carboxylic acids for carbodiimide immobilization of capture agents such as antibodies.

with active CTAs continue to extend. Polymerization was conducted in the presence of a primary amine, butylamine, that is protonated and unreactive during S-RAFT polymerization at pH 4.5. To establish the first layer, the pH is temporarily raised to 11 with NaOH, which deprotonates butylamine for partial CTA aminolysis. To create the sparse second layer, the pH is returned to 4.5 (by adding 12 M HCl) before complete CTA aminolysis. The bimodal pCB surfaces resisted non-specific protein adsorption (<6.7 ng cm^{-2}) and decreased macrophage adhesion. Compared to brush only layers, the bimodal pCB layers increased antibody, capture agent, loading 5-fold and improved the capture of biotin-fluorescein on avidin modified layers by 4-fold.

2. Materials and methods

2.1. Materials

N-[3-(Dimethylamino)propyl]methacrylamide, *tert*-butyl bromoacetate, trifluoroacetic acid (TFA), 4-cyano-4-(phenylcarbonothioylthio)pentanoic acid, 4,4′-azobis(4-cyanovaleric acid), sodium dodecyl sulfate (SDS), (3-aminopropyl) triethoxysilane (APTES), *N*,*N*′-diisopropylcarbodiimide (DIC), *N*-(3-dimethylaminopropyl)-*N*′-ethylcarbodiimide hydrochloride (EDC), *N*-hydroxysuccinimide (NHS), sodium hydroxide (NaOH), QuantiPro™ BCA Assay Kit, sodium acetate, bovine serum albumin (BSA), Biotin (5-fluorescein) conjugate (biotin-fluorescein), TWEEN® 20, were purchased from Sigma Aldrich (Oakville, ON, Canada). Methanol, toluene, dichloromethane (DCM), diethyl ether, 1,4-dioxane, dimethylformamide (DMF), hydrochloric acid (HCl), sulfuric acid, and acetic acid were purchased from Caledon (Georgetown, ON, Canada). Alexa Fluor® 647 NHS ester, calf bovine serum (CBS) and fetal bovine serum (FBS), calcein AM, HOESCHT stain, trypsin and avidin were obtained from Thermo Fisher Scientific (Burlington, ON, Canada). Dulbecco's modified Eagle medium (DMEM) was purchased from Corning (Tewksbury, MA, USA). Silicon wafers were purchased from University Wafers (Boston, MA, USA). Bevacizumab was provided by Boston Children's Pharmacy (Boston, MA, USA). Phosphate buffered saline (PBS) at pH 7.4 contained 10 mM sodium phosphate and 137 mM NaCl.

Carboxybetaine methacrylamide (CB) monomer was synthesized *via* a previously published method.[17] Briefly, 23.25 g (136.5 mmol, 1 equiv.) of *N*-[3-(dimethylamino)propyl]methacrylamide was dissolved in 300 mL of dry acetonitrile under N_2. *tert*-Butyl bromoacetate (30 g, 153.8 mmol, 1.1 equiv.) was added, and left to react overnight at 50 °C. The reaction was cooled to room temperature and the product was precipitated with 500 mL of ether. The product was left to stand at 4 °C overnight, and decanted. The white powder was collected, washed with 100 mL of ether, decanted, and dried under a stream of nitrogen, followed by incubation overnight under vacuum. The *t*-butyl protected intermediate was then deprotected by dissolving in neat TFA and incubating at room temperature for 2 h. The deprotected CB monomer was precipitated in ether, dried under a nitrogen stream, and freeze drying. ^{1}H NMR (D_2O, 600 MHz) δ: 5.63 (s, 1H), 5.34 (s, 1H), 4.10

(s, 2H), 3.53 (m, 2H), 3.28 (t, $J = 6.42$, 2H), 3.18 (s, 6H), 1.96 (m, 2H), 1.85 (s, 3H).

Fluorescent bevacizumab (bevacizumab-647) was synthesized by mixing 7.5 μL Alexa fluor-647 NHS DMF solutions (10 mg mL^{-1}; 0.075 mg, 0.06 μmol, 3 equiv.) with 100 μL of a bevacizumab solution (3 mg, 0.02 μmol, 1 equiv.) in PBS (pH 7.4) for 3 h in the dark. Bevacizumab-647 was purified by dialysis (MWCO 12–14 kDa) against PBS at 4 °C in the dark. The final bevacizumab-647 concentration and substitution ratio (dyes per antibody) was calculated from absorbance measurements taken with a Biotek Cytation 5 plate reader equipped with a Take3 micro-volume plate using extinction coefficient for Alexa fluor-647 of 239 000 cm^{-1} M^{-1} and a correction factor of 0.03.

2.2. Modification of silica surfaces

2.2.1. Modification of silica surfaces and APTES deposition. Silicon wafers (100 mm, N-type, ⟨100⟩, 1–10 ohm cm) were soaked in 1 : 1 HCl : methanol for 30 min, rinsed with Milli-Q water and dried under nitrogen. The wafers were then soaked in concentrated H_2SO_4 for 30 min, rinsed with Milli-Q water and dried under a stream of nitrogen. Surfaces were then spin coated with a 0.1% v/v APTES in dry toluene (dried over 3 Å molecular sieves), sonicated for 1 min in dry toluene, dried under a stream of nitrogen, and incubated for 1 h at 70 °C.

2.2.2. Immobilization of RAFT chain transfer agent. 4-Cyano-4-(phenylcarbonothioylthio)pentanoic acid (14 mg, 0.05 mmol, 1 equiv.) was activated with DIC (39 μL, 0.25 mmol, 5 equiv.) and NHS (29 mg, 0.25 mmol, 5 equiv.) in DCM (1 mL; dried over 3 Å molecular sieves) and stirred overnight at room temperature under nitrogen. APTES functionalized silica wafers were then added to the DCM solution, diluted to 5 mL, which was then kept under nitrogen for 60 h with gentle stirring.

2.3. Solution and graft-from polymerizations

2.3.1. Synthesis of pDMAPMA. Bimodal pDMAPMA distributions in solution were synthesized as follows. *N*-[3-(Dimethylamino)propyl]methacrylamide monomer (1.3 mL, 7.8 mmol, 130 equiv.), 4-cyano-4-(phenylcarbonothioylthio) pentanoic acid (15.4 mg, 0.05 mmol, 1 equiv.), 4,4′-azobis(4-cyanopentanoic acid) (7.7 mg, 0.27 mmol, 0.5 equiv.) and butylamine (50 μL, 0.5 mmol, 9 equiv.) were dissolved in 5 mL of 2 : 1 acetate buffer (0.1 M, pH 4.5) and 1,4-dioxane. The pH was adjusted to 4.5 with NaOH (8 M) and degassed *via* three freeze–pump–thaw cycles with nitrogen backfills and incubated at 70 °C with gentle stirring. Two different bimodal polymerizations were performed: (1) after 2 h at 70 °C, an aliquot of polymerization solution was removed for gel permeation chromatography (GPC) characterization and degassed NaOH (8 M, 500 μL) was added to the reaction vessel to raise the pH and initiate CTA aminolysis. After 6 min at high pH, HCl (12 M, 335 μL) was added to end aminolysis and the polymerization was maintained for 22 h. And, (2) after 4 h at 70 °C, an aliquot of polymerization solution was removed for GPC characterization and degassed NaOH (8 M, 500 μL) was added to the reaction vessel to initiate CTA aminolysis. After 6 min at high pH, HCl (12 M, 335 μL) was then added to end aminolysis and polymerization was maintained for 20 h.

Trimodal pDMAPMA was synthesized similarly to the bimodal pDMAPMA polymerization described in condition 1 above, except degassed NaOH (8 M, 500 μL) was also added after 9 h polymerizaton, and HCl (12 M, 335 μL) at 9 h and 6 min, with a total polymerization time of 45 h.

2.3.2. Synthesis of bimodal solution and graft-from pCB. Solution polymerization is simultaneously occurring during graft-from synthesis of pCB layers, we therefore performed the same procedure for solution and graft-from polymerizations. CB monomer (1.5 g, 6.6 mmol, 130 equiv.), 4-cyano-4-(phenylcarbonothioylthio)pentanoic acid (14.1 mg, 0.05 mmol, 1 equiv.), 4,4′-azobis(4-cyanopentanoic acid) (7.1 mg, 0.025 mmol, 0.5 equiv.) and butylamine (50 μL, 0.5 mmol, 10 equiv.) were dissolved in 5 mL 2 : 1 acetate buffer (0.1 M, pH 4.5) and 1,4-dioxane. The pH was adjusted to 4.5 with NaOH (8 M) and a CTA functionalized silicon wafer was submerged in the polymerization solution. The solution was degassed *via* three freeze–pump–thaw cycles, backfilled with nitrogen and incubated at 70 °C for 1 h with gentle stirring. After 1 h, an aliquot of polymerization solution was removed for GPC characterization and degassed NaOH (8 M, 500 μL) was added to the reaction vessel to initiate aminolysis. After 5 min at high pH, HCl (12 M, 335 μL) was added to end aminolysis and the solution was reacted for an additional 23 h.

2.3.3. GPC characterization of solution polymers. Polymer molecular weights (M_n, M_w) and dispersity ($Đ$) were determined by GPC using an Agilent 1260 infinity II GPC system equipped with an Agilent 1260 infinity RI detector, and either a Superpose 6 increase 10/300 GL (GE healthcare) column (bimodal pDMAPMA, pCB with and without butylamine), Superose 6 increase 10/300 GL and HiLoad 16/600 Superdex 200 pg (GE healthcare) columns in series (trimodal pDMAPMA), or PL aquagel-OH 30 and PL aquagel-OH 40 (Agilent) columns in series (monomodal pCB) with PBS running buffer at 30 °C. Columns were calibrated using polyethylene glycol (PEG) standards (M_n of 3000 to 60 000 Da).

GPC chromatograms of bimodal pCB were deconvolved with Microsoft Excel assuming two peaks fit as normal Gaussian distributions using the included generalized reduced gradient (GRG) nonlinear algorithm. The ratio of high to low molecular weight polymers in bimodal distributions were calculated as the relative ratio of the area of these Gaussian distributions.

2.4. Surface characterization

2.4.1. Ellipsometry. Film thickness measurements were obtained using an M-2000UI (J.A. Woolam) variable angle spectroscopic ellipsometer at 55 to 75° in 5° increments with light spectrum from 250 to 1680 nm. All films were modeled as transparent single layer Cauchy films with no surface roughness on Si substrates with the CompleteEase Software package.

2.4.2. X-ray photoelectron spectroscopy. Modified wafers were analyzed with a PHI Quantera II scanning X-ray photoelectron spectroscopy (XPS) microprobe. A take-off angle of 45° was used for all samples, pass energy and step size were 224 eV

and 0.8 eV for survey scans and 55 eV and 0.1 eV for high resolution scans, which were used to determine elemental composition.

2.4.3. Water contact angle. Static water contact angle (WCA) measurements and images were acquired with an OCA 20 (Future Digital Scientific) contact angle measurement system and calculated with the SCA 20 software module. 3 μL droplets of Milli-Q water were deposited on APTES functionalized, CTA functionalized, and 1 and 2 layer pCB surfaces.

2.5. Modification of pCB surfaces with capture agents

2.5.1. Bevacizumab-647 immobilization. 1 and 2 layer pCB wafers were activated for protein immobilization *via* incubation in 200 μL of a 0.2 M EDC (76.7 mg, 0.4 mmol, 1 equiv.) and 0.05 M NHS (11.5 mg, 0.1 mmol, 0.25 equiv.) water solution for 7 minutes at 4 °C. The wafers were then rinsed with a sodium acetate buffer (0.1 M, pH 4.5), placed in a 200 μL solution of bevacizumab-647 (500 μg mL^{-1}) in PBS, and incubated for 20 min at 4 °C in the dark. Wafers were then water bath sonicated in fresh PBS 3 times for intervals of 1 min to remove excess protein. Surface fluorescence microscopy imaging was performed with a Biotek Cytation microscope, equipped with a Cy5 filter set. Intensity quantification was performed with the ImageJ Mean Gray Value tool. Surface fluorescence values were converted to ng cm^{-2} by comparison with a calibration curve of dropcast bevacizumab-647 of known total mass onto wafers and imaged under the same conditions as experimental samples to produce a calibration curve.

2.5.2. Avidin immobilization and biotin fluorescein capture. Avidin was immobilized onto 1 and 2 layer pCB using the same procedure as bevacizumab-647. Following immobilization, surfaces were rinsed 6 times with 0.05% TWEEN 20 in PBS (PBS-T). Avidin functionalized wafers and pCB coated wafers without avidin were incubated in 100 μL of 4 μg mL^{-1} biotin-fluorescein in PBS for 2 h in the dark under agitation (orbital shaker at 100 RPM). The biotin-fluorescein solution was removed and surfaces were rinsed 6 times with PBS-T. Fluorescence of each well was measured with a Biotek Cytation plate reader and surface fluorescence was imaged by fluorescent microscopy. Surface fluorescence values were converted to ng cm^{-2} by comparison with a calibration curve of dropcast biotin-fluorescein of known total mass onto wafers and imaged under the same conditions as experimental samples.

2.6. Characterization of protein and macrophage fouling on pCB coated surfaces

2.6.1. Non-specific protein fouling. Total non-specific protein adsorption was measured by a bicinchoninic acid (BCA) assay of collected protein, as previously reported.[18–20] Pristine silicon, 1 and 2 layer pCB, and pDMAPMA surfaces were incubated with 100% aged CBS at 37 °C for 1 h. Following incubation, the wafers were rinsed with deionized (DI) water and incubated in PBS for 15 min on an orbital shaker table at 100 RPM. The wafers were then removed from the PBS solution and dried under a stream of nitrogen. To extract adsorbed protein from the dry wafers, 120 μL of 8% SDS in deionized (DI) water was added to cover the surface, the wafers were then incubated in a humidity chamber overnight at 37 °C. The SDS solution was removed from the wafers and incubated for 2 h at 37 °C with BCA assay kit reagents as per manufacturer protocol.[21] Finally, absorbance was read at 562 nm and compared against a BSA calibration curve to determine the total adsorbed protein content. The total amount of protein in the SDS solution was then determined using the BCA protein quantification assay with a calibration curve. The calibration curve was prepared using BSA calibrants in the SDS solution used to remove adsorbed protein from wafers. The lowest detectable concentration in the BSA calibration curve was 0.3 μg mL^{-1}. The SDS solutions used for BSA extraction were 120 μL and the wafers were 5.4 cm^2. Therefore, the limit of detection (LOD) is equal to:

$$\begin{aligned}\mathrm{LOD} &= \frac{\text{total BSA absorbed}}{\text{wafer surface area}} \\ &= \frac{\text{lowest detectable [BSA]} \times \text{volume of SDS solution}}{\text{wafer suface area}} \\ &= \frac{0.3\ \mu g\ mL^{-1} \times 0.12\ mL}{5.4\ cm^2} \\ &= 6.7\ ng\ cm^{-2}\end{aligned}$$

2.6.2. Non-specific macrophage adhesion. pCB coated silicon wafers were placed into a 96 well plate. Wells were soaked in 70% ethanol for 1 h to sterilize the surfaces. The ethanol was removed and each wafer was rinsed three times with water, and incubated for 24 h with 200 μL of FBS at 37 °C. FBS was removed and 200 μL of RAW 264.7 macrophages (50 000 cells per mL) in DMEM supplemented with 10% FBS were added to each well and cultured for 2 d at 37 °C and 5% CO_2. Cell media was then removed, and each well was rinsed three times with 37 °C PBS. Cells were stained with calcein AM and HOESCHT according to manufacturer protocols. Silicon wafers were imaged with a Biotek Cytation fluorescent microscope equipped with DAPI and GFP filter cubes, and cells with colocalized stains were counted.

2.7. Statistical methods

All graphed data represents mean ± standard deviation calculated from triplicate measurements, unless otherwise stated. All statistical analysis was performed using GraphPad Prism 8. $P < 0.05$ is indicated by *, $P < 0.01$ by **, and $P < 0.001$ by ***.

3. Results and discussion

3.1. Demonstration of pH-controlled RAFT polymerization in solution: synthesis of multimodal pDMAPMA and pCB

To demonstrate the production of multimodal polymer distributions using pH-controlled RAFT, we first conducted and characterized the solution polymerization of pDMAPMA and pCB, using a thiocarbonylthio containing CTA end group at the polymer's living end. Controlled partial degradation of the thiocarbonylthio group, which prevents further monomer addition, led to bi- or multi-modal polymer M_w distributions. Here,

we reacted a fraction of polymer thiocarbonylthio end groups with an amine nucleophile, butylamine, to yield terminal thiols and a thioamide side product (Scheme S1†).

Partial termination of CTAs with amino nucleophiles allows for one-pot synthesis of bimodal polymer M_w distributions by temporarily raising the pH; the amine is protonated and unreactive at pH 4.5, and unprotonated and reactive at pH 11. Butylamine was chosen as the nucleophile because it is soluble under pCB's aqueous polymerization conditions and has a pK_a of ~10.5,[22] which minimizes aminolysis during pH 4.5 RAFT polymerization.[23,24] A 10-fold molar excess of butylamine compared to CTA agent during polymerization ensured efficient aminolysis at high pH. The elapsed polymerization time prior to pH raising determined the M_w of the low M_w polymer population.

Two different bimodal pDMAPMAs were synthesized with partial aminolysis at 2 or 4 h after initiation; polymers were characterized by GPC (Fig. 2A) and NMR (Fig. S1B†). The low M_w polymer population increased from 8.0 to 9.2 kDa as polymerization time prior to aminolysis increased from 2 to 4 h, minimal differences in $Đ$ were observed (1.03 *versus* 1.05; Table 1). We also confirmed that pDMAPMA's tertiary amine does not result in CTA aminolysis at pH 4.5 (Fig. S2†). The ability to synthesize multimodal distributions was further tested by synthesizing a trimodal distribution of pDMAPMA with partial aminolysis at 2 and 9 h, and a total polymerization time of 45 h. This resulted in the production of three distinct M_w populations of 7 ($Đ = 1.02$), 70, and 391 kDa, respectively; the dispersity of the two high M_w populations could not be accurately calculated due to elution near the exclusion limit of the column (Fig. 2B).

To determine the duration of aminolysis required for pCB bimodal distributions, pCB was synthesized with pH 11 intervals of 5, 30 or 60 min. The 5 min interval yielded a clear bimodal distribution according to GPC analysis, with two M_w populations of 6.5 ($Đ = 1.02$) and 10.5 kDa ($Đ = 1.11$) (Table 1, Fig. 3A); the bimodal solution was further characterized by NMR (Fig. S1A†). The 30 and 60 min intervals most likely resulted in maximum aminolysis of the CTAs and uncontrolled polymerization of propagating chains, which resulted in bimodal distributions dominated by the low M_w population (Fig. 3). To determine the

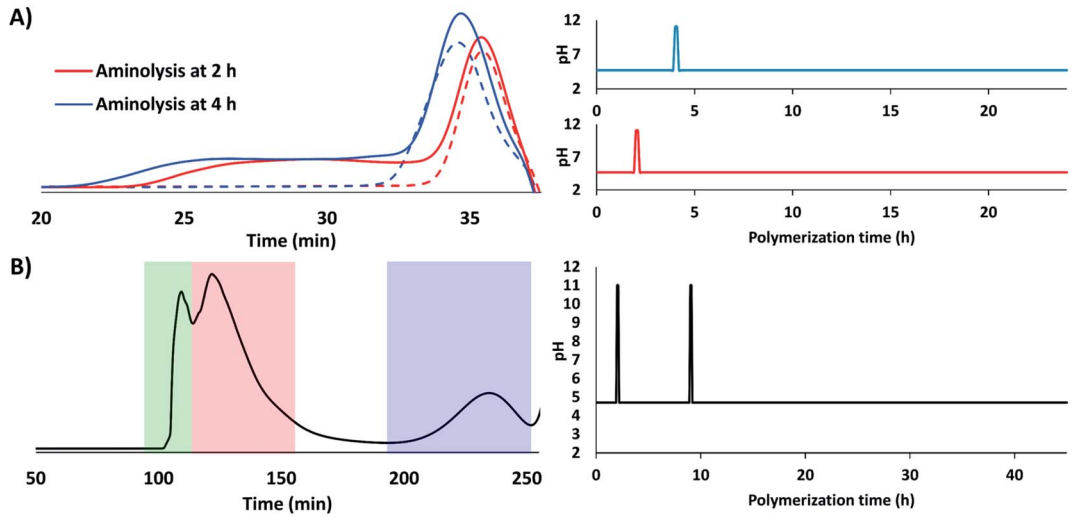

Fig. 2 GPC analysis of multimodal distributions from solution polymerization of pDMAPMA using pH-controlled RAFT. pH time courses during polymerizations are plotted on the right. (A) GPC analysis of two different pDMAPMA polymerizations with partial CTA aminolysis at 2 (red) or 4 h (blue), respectively, by temporarily raising the pH for 5 min. GPC analysis prior to pH raising (dashed lines) demonstrated that pH raising is required for multimodal distributions. (B) pDMAPMA polymerization with sequential 6 min partial CTA aminolysis at 2 and 9 h resulted in three distinct M_w populations highlighted in blue, red and green.

Table 1 Characterization of low and high M_w populations in bimodal solution polymerizations

Polymer[a]	Aminolysis duration (min)	Low M_w population			High M_w population		
		M_w (kDa)	M_n (kDa)	$Đ$	M_w (kDa)	M_n (kDa)	$Đ$
$pDMAPMA_{2h}$	5	8.0	7.8	1.03	32.5	25.0	1.30
$pDMAPMA_{4h}$	5	9.2	8.8	1.05	43.8	32.4	1.35
pCB_{1h}	5	6.4	6.5	1.02	9.5	10.5	1.11
pCB_{1h}	30	6.4	6.5	1.02	8.8	9.4	1.07
pCB_{1h}	60	6.4	6.7	1.04	10.0	10.8	1.08

[a] Subscript indicates polymerization time prior to pH raising.

relative distribution of low and high M_w populations, the GPC data was deconvolved assuming Gaussian distribution to yield a 0.43 : 0.57 ratio of low to high M_w populations for the 5 min pH 11 time interval. Deconvolution of GPC traces of conditions with 30 and 60 min at pH 11 yielded greater proportions of the low M_w population, as expected. To ensure aminolysis is required for bimodal polymerization, the pCB synthesis protocol was repeated in the absence of butylamine; no clear bimodal pCB distributions were observed in the absence of butyl amine (Fig. S3†). Therefore, bimodal populations of pCB can be synthesized using pH-controlled RAFT with butylamine and a pH 11 interval of 5 min. Because the monomer must be stable under basic conditions for pH controlled aminolysis, CB with a 1 carbon spacer length (CSL) between charges was chosen; CBs with a CSL of 2 have been reported to undergo elimination reactions under basic conditions.[25] We confirmed that no pCB structure modifications occurred upon exposure to high pH aminolysis conditions by NMR (Fig. S1†).

3.2. Graft-from pCB synthesis on silicon wafer surfaces was confirmed by XPS

Using XPS, we first confirmed that the silicon wafers were activated with CTA agent and amenable to graft-from polymerization of pCB. Silicon wafers were spin coated with APTES and reacted with CTA's carboxylic acid using DIC to form an unreactive amide bond towards aminolysis. XPS of the wafers confirmed the presence of nitrogen and sulfur after immobilization of APTES and CTA, respectively, which indicates successful surface functionalization. The wafers were then immersed in a pCB polymerization solution that was then heated to initiate concurrent solution and surface pCB polymerization. After polymerization, the pCB modified wafers had greater carbon content compared to CTA modified surfaces according to XPS (Table 2). Therefore, the CTA modified wafers are amenable to pCB graft-from polymerization.

3.3. Graft-from synthesis of bimodal pCB through pH-controlled S-RAFT

The synthesis of bimodal pCB surfaces using pH-controlled S-RAFT was confirmed through WCA, spectral ellipsometry, and

Table 2 XPS derived elemental composition of pristine and modified silicon wafers[a]

	Atom%				
Sample	C	O	N	S	Si
Pristine	4.4	44.8	—	—	50.8
APTES	13.9	40.9	2.7	—	42.5
CTA	26.9	38.2	5.8	2.2	27
1 layer pCB	50	23.9	4.3	2.1	19.7

[a] 1 layer pCB had a thickness of 12.6 ± 2.7 nm.

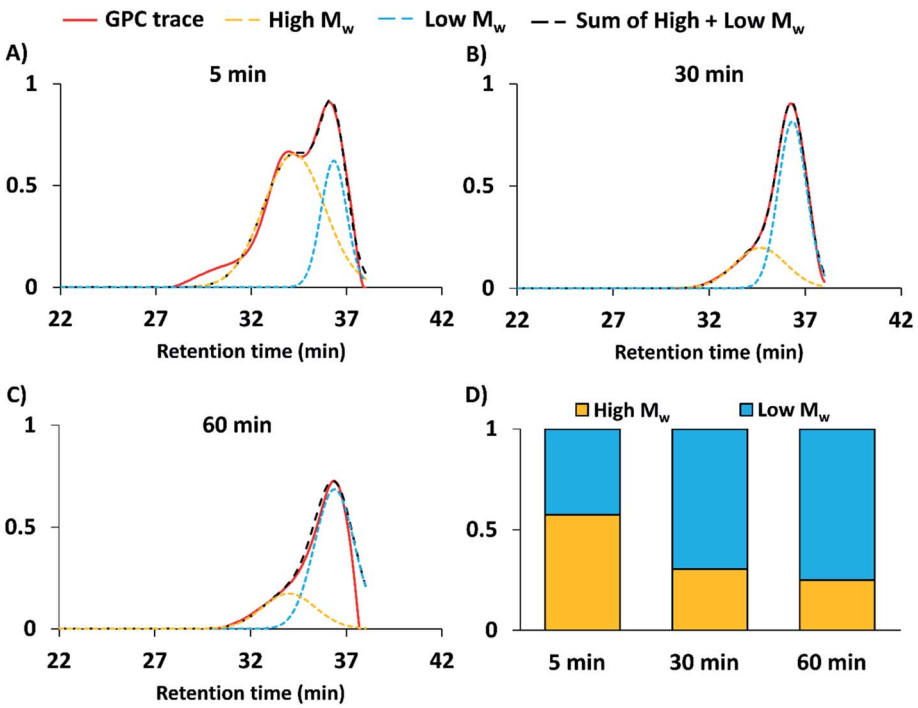

Fig. 3 Dependence of pH 11 time interval on pCB's bimodal M_w distributions in the presence of butylamine. GPC traces (red line) of bimodal pCB polymerizations conducted as follows: (1) pH was held at 4.5 for 1 h; (2) pH was temporarily raised to 11 for (A) 5, (B) 30 and (C) 60 min, respectively; and, (3) pH was returned to 4.5 for a total polymerization time of 24 h. Dashed lines represent deconvolution of GPC data as Gaussian distributions to separate high (yellow) and low (blue) M_w populations; the black dashed line represents the sum of the deconvoluted high and low M_w populations. (D) Calculated proportions of high and low M_w polymer populations from deconvolution. Control experiments without butylamine are presented in Fig. S3.†

protein loading. Bimodal pCB layers were successfully polymerized with a 5 min pH 11 interval after 1 h of polymerization, as described in Section 3.1. As controls, 1 layer pCB wafers were prepared with a total polymerization time of 1 h at pH 4.5.

To follow each surface modification step, the WCA of the wafers was measured after APTES, CTA, 1 layer pCB and 2 layer pCB synthetic steps. APTES modified surfaces demonstrated a WCA of ~40° that is characteristic of an aminosilane monolayer on silicon surfaces,[26] where the amines are orientated away from the surface with all three ethoxy groups reacted. CTA functionalized surfaces demonstrated WCAs (~55°) typical of CTA, 4-cyano-4-(phenylcarbonothioylthio)pentanoic acid, monolayers.[27] The WCA of pCB modified surfaces is dependent on the degree of polymerization;[28] therefore, 2 layer (bimodal) pCB surfaces with a 24 h polymerization time had a lower WCA than 1 layer pCB surfaces with a 1 h polymerization time. The WCA of the bimodal architecture (~10°) is hydrophilic and equivalent to the those previously reported for thick pCB layers.[29] The high variability in WCA for 1 layer pCB modified wafers (standard deviation of 10, Fig. 4A) is characteristic of thin coatings due to the sensitivity of WCA measurements to slight film thickness variations.[28] To demonstrate that polymerization time (*i.e.* degree of polymerization) influences WCA measurements, the WCA of unimodal and bimodal pCB surfaces produced using a 24 h polymerization timed had similar WCAs (Fig. 4A and S4†).

The greater thickness of 2 layer pCB architectures compared to 1 layer pCB was confirmed by spectral ellipsometry of dry pCB films. The average thickness of the 2 layer coating was ~2.4 times greater than the 1 layer coating (Fig. 4B), due to the formation of the low-density second layer. The layer thickness increased at each modification step from the native oxide layer on the silicon wafer, APTES, CTA, 1 layer pCB and 2 layer pCB (Fig. 4B), indicating a successful modification procedure.

The 2 layer pCB architecture was also confirmed to have greater antibody loading potential through the immobilization of a fluorescent antibody, bevacizumab modified with Alexa 647 (Fig. 5). Bimodal pCB layers have previously been shown to increase the surface capacity of immobilized antibodies when compared to monomodal brush pCB layers, where thicker low density layers lead to greater loading levels.[16] High-density monomodal polymer layers demonstrate lower degrees of protein immobilization because high-density of polymer chains prevent biomacromolecule diffusion.[30] Using EDC/NHS chemistry to activate pCB carboxylic acids, Alexa 647 modified bevacizumab was immobilized onto monomodal brush and bimodal pCB surfaces. Wafers were then characterized by surface fluorescence, which indicated ~5-fold greater bevacizumab immobilization on bimodal surfaces. Therefore, bimodal pCB surfaces produced through pH controlled S-RAFT retained the advantageous property of greater capture agent immobilization.

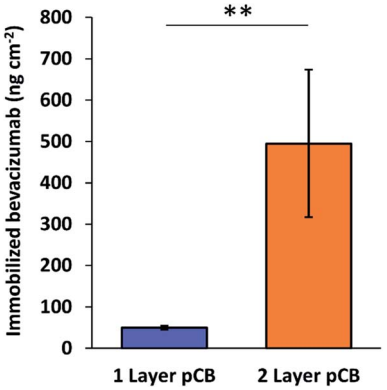

Fig. 5 Immobilization of bevacizumab confirmed the greater loading capacity of bimodal pCB wafers. Fluorescently labelled bevacizumab was immobilized using EDC/NHS chemistry on 1 (brush) and 2 layer (bimodal) pCB wafers. After quantification by fluorescent microscopy, the 2 layer pCB architecture was confirmed to have a higher loading capacity than 1 layer pCB. $P < 0.01$ (**), by Student's t-test, mean ± standard deviation.

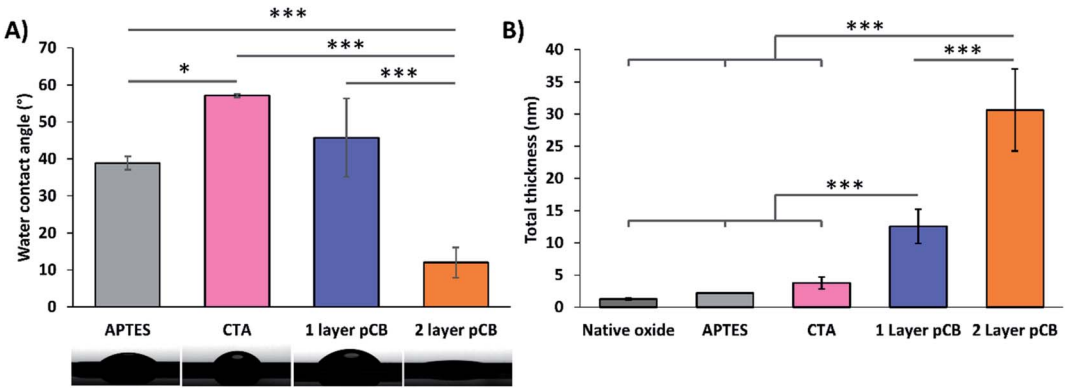

Fig. 4 Surface characterization of functionalized silicon wafers by WCA and ellipsometry. (A) Static WCA and representative photographs of 3 μL water droplets on wafers functionalized with aminosilane, CTA, and 1 and 2 layer pCB coatings. Hydrophobic CTA increased the WCA contact, whereas increasing pCB content decreased the WCA. The WCA of 1 layer pCB was greater than 2 layer pCB due to differences in layer thickness. (B) Modeled layer thickness of native oxide, APTES, CTA, and 1 and 2 layer pCB coatings from spectral ellipsometric measurements. Statistics performed by one-way ANOVA with Bonferroni's multiple comparison test (mean ± standard deviation $p < 0.05$ (*), and $p < 0.001$ by (***)).

3.4. Avidin modified bimodal pCB surfaces enhanced biotin capture

Bimodal pCB layers functionalized with avidin captured approximately 4 times more biotin-fluorescein than avidin modified brush pCB surfaces (Fig. 6). The improved capturing capacity is similar to previously reported bimodal polymer surfaces which increased capacity by 1.8 to 3.1 times.[9,15] Avidin was first immobilized on the pCB surfaces using EDC/NHS chemistry. The surfaces were then incubated in biotin-fluorescein solutions for 2 h, then extensively washed to remove unbound biotin. Fluorescence microscopy was performed on biotin-fluorescein exposed 1 and 2 pCB layer surfaces with and without immobilized avidin (Fig. 6B). The bimodal 2 layer pCB surfaces with avidin had greater total fluorescence intensity, which indicates a greater amount of captured biotin-fluorescein compared to 1 layer pCB surfaces. Quantitative surface fluorescence measurements indicated ~4-fold increase in biotin-fluorescein capture on bimodal (2 layer) architectures when compared to brush (1 layer) surfaces (Fig. 6C); surfaces without avidin were used as background controls. Therefore, bimodal architectures improved both capture agent immobilization and target molecule binding.

3.5. pCB surfaces prepared by pH-controlled RAFT are low-fouling

1 and 2 layer pCB architectures had similar low-fouling properties due to the pCB brush architecture present on both surfaces. pCB coatings synthesized by the graft-from method are employed to generate low-fouling surfaces towards proteins, which has been defined as below 5 ng cm^{-2};[31] whereas, surfaces prepared by graft-to methods exposed to undiluted serum non-specifically adsorb proteins at 11 ng cm^{-2}.[32] In this study, 1 and 2 layer pCB architectures were exposed to 100% aged CBS to evaluate protein fouling in complex media relevant for biological applications; aged serum has been shown to foul surfaces to a greater degree than fresh serum.[33] pCB surfaces were compared to positive fouling controls of cationic pDMAPMA modified surfaces and anionic plasma cleaned SiO_2 wafers. All surfaces were incubated in CBS for 1 h and washed extensively in PBS prior to adsorbed protein quantification using an SDS extraction method and the BCA protein quantification assay, as previously described.[20] Adsorbed protein on the 1 and 2 layer pCB surfaces was below the assay detection limit of 6.7 ng cm^{-2}, while the pDMAPMA control surface had ~130 ng of adsorbed protein per cm^{-2} (Fig. 7A). The calculated values of adsorbed

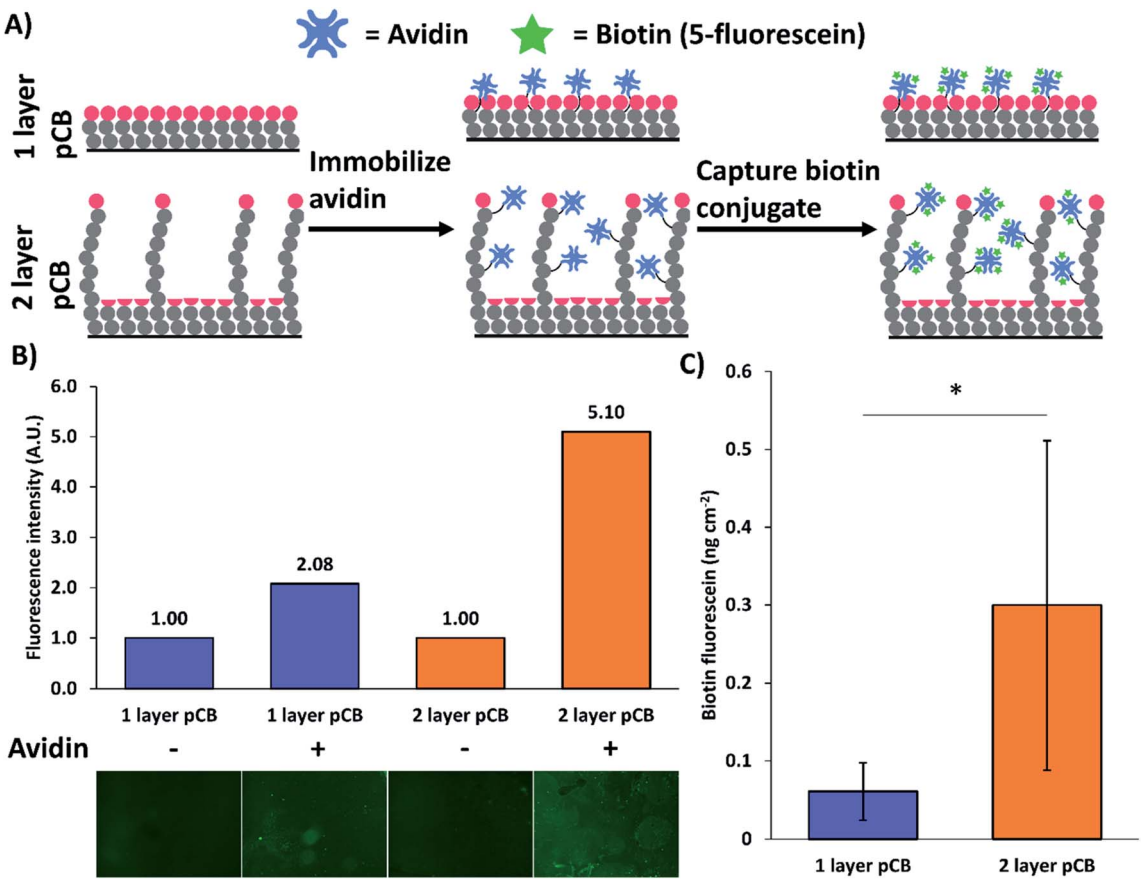

Fig. 6 Bimodal, two layer, pCB wafers modified with avidin have greater biotin capturing efficiency. (A) Schematic for the modification of pCB surfaces with avidin and subsequent biotin-fluorescein capture. (B) Representative fluorescent micrographs (4× magnification) and micrograph fluorescent intensity from 1 and 2 layer pCB surfaces with and without avidin that were exposed to biotin-fluorescein. (C) Surface fluorescence quantification of biotin-fluorescein bound to avidin modified surfaces ($n = 5$ for 1 layer pCB, $n = 6$ for 2 layer pCB, mean ± standard deviation, $p < 0.05$ (*), Student's t-test). Background signal was removed by measuring fluorescence of avidin-free surfaces after exposure to biotin-fluorescein.

protein assumed complete extraction with SDS, which has been shown to not hold for all protein interactions,[34] and thus represent lower bounds. Nonetheless, 1 and 2 layer pCB coatings were demonstrated to improve protein fouling resistance. The relative decrease in detected absorbed protein between control surfaces and pCB coatings is similar to previously reported values using the SDS BCA assay (~20×).[35,36] Therefore, bimodal pCB surfaces synthesized by pH-controlled S-RAFT resist protein fouling to a similar extent as previously reported bimodal architectures synthesized by SI-ATRP and SI-PIMP.

Surface fouling was further characterized by quantifying non-specific macrophage adhesion to serum exposed surfaces. Both 1 and 2 layer pCB coatings reduced macrophage adhesion by >90% when compared to tissue culture plastic (TCP) and plasma cleaned wafers (SiO_2; Fig. 7B and C). To ensure maximum macrophage binding, all surfaces were pre-incubated in FBS for 24 h prior to cell seeding (10 000 macrophages per surface). After seeding, surfaces were cultured for an additional 2 d to promote maximum macrophage adhesion to identify potential difference in nonspecific macrophage adhesion. Surfaces were then gently washed with PBS and cells were stained with HOESCHT and calcein AM for counting. Both 1 and 2 layer pCB decreased macrophage adhesion to a similar extent (Fig. 7B and C), indicating both surfaces had similar low-fouling properties towards cells, as expected.

3.6. Further discussion

pH-Controlled bimodal S-RAFT polymerization simplifies the synthesis of bimodal pCB layers and avoids the use of potentially toxic materials (*e.g.* Cu), increasing the accessibility of bimodal pCB surfaces for incorporation into sensors and medical devices. Bimodal architectures were achieved by the temporal control of pH (through NaOH and HCl additions) to temporarily deprotonate butylamine for partial CTA aminolysis. The method can be extended to other CTAs due to the standard thiocarbonylthio bond found in many RAFT CTAs,[37] enabling polymerization of monomers that may not be compatible with 4-cyano-4-(phenylcarbonothioylthio)pentanoic acid. This technique can further be extended to other substrate materials such as gold, an important substrate for biosensors, as only the initial amine functionalization chemistry must be adapted; S-RAFT has previously been performed on gold surfaces.[38]

The development of high loading, low-fouling surfaces is particularly important for biomedical sensors and blood

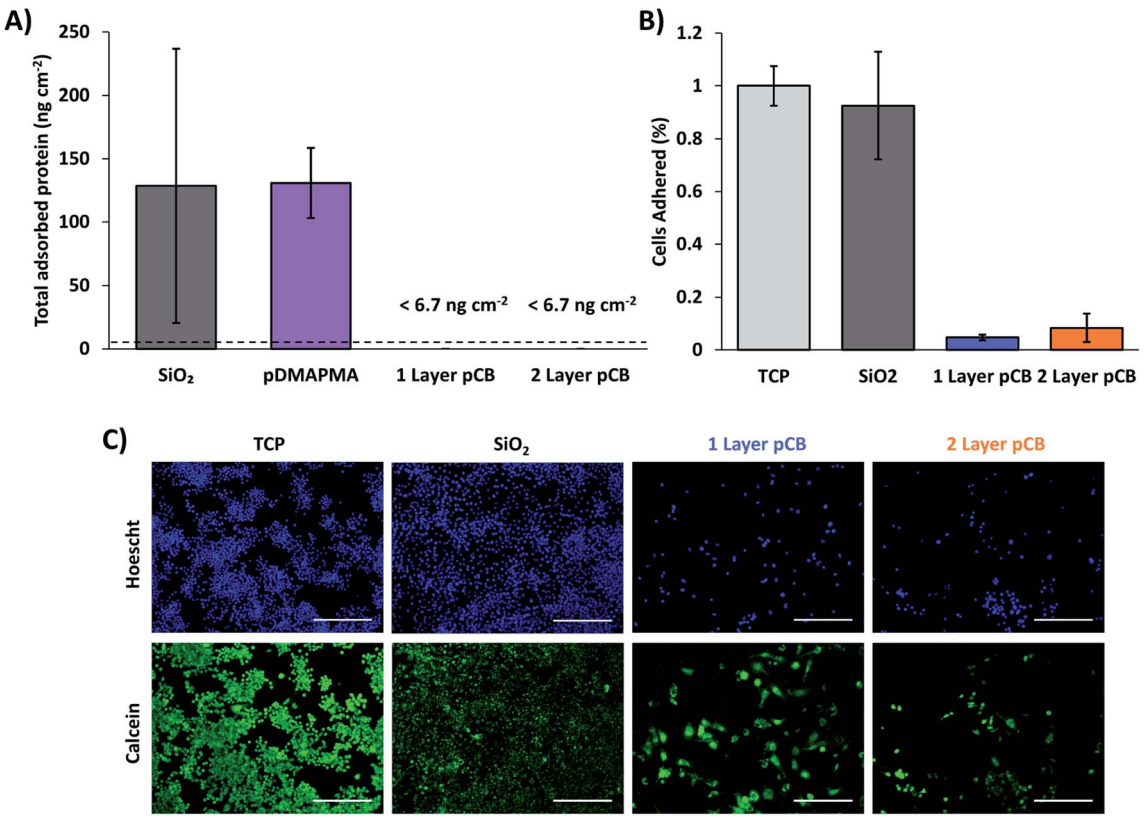

Fig. 7 One and two layer pCB surfaces were equally low-fouling when exposed to serum. (A) Non-specific protein adsorption onto pristine silicon wafers and wafers functionalized with single layers of pDMAPMA and pCB, and bimodal pCB when incubated in CBS for 24 h; cationic pDMAPMA and anionic SiO_2 surfaces were included as a positive fouling control. No adsorbed protein was detected on 1 or 2 layer pCB (detection limit of the assay was 6.7 ng cm^{-2}); protein adsorption was therefore comparable to non-fouling surfaces.[31]. (B) After 48 h of culturing, relative amounts of adhered macrophages on surfaces pre-exposed to serum for 24 h was quantified. Cell counts were determined from fluorescent micrographs; numbers were normalized to the tissue culture plastic (TCP) control. (C) Representative fluorescent micrographs of adhered macrophages stained with HOESCHT and calcein AM, scale bars = 200 μm.

purification devices. The ability to rapidly detect cytokines in blood or tissue extracts is increasingly important due to the development of immune modulating drugs such as cancer immunotherapies, where cytokine levels are carefully tracked.[39] Recently, the development of polymeric surfaces for blood cytokine[40] and lipopolysaccharide[41] (LPS) filtration has shown promise for the treatment of sepsis; cytokine filtration could also have applications in cardio-renal syndromes.[42] Blood filtration with low-fouling bioactive surfaces can selectively alter blood biochemistry with temporal control by administering in-line filters to patients.[43]

4. Conclusions

The development of low-fouling surfaces that selectively capture molecules from biological fluids is crucial in the development of biosensors and blood filtration devices. We developed pH-controlled S-RAFT to simplify the synthesis of bimodal pCB layers that increase capturing efficiency while retaining low-fouling properties. Compared to monomodal pCB architectures, bimodal surfaces improved capture agent, antibody, immobilization and target molecule, biotin-fluorescein, capture by 4 to 5-fold. pH-Controlled S-RAFT only requires a temporary increase in pH for CTA aminolysis during surface preparation, which will help towards increasing the accessibility of bimodal architectures for biomedical applications.

Conflicts of interest

There are no conflicts to declare.

Acknowledgements

This work was supported by the Natural Sciences and Engineering Research Council (NSERC; 2015-05429), Canada Foundation for Innovation: John R. Evans Leaders Fund (CFI-JELF; 34107), Ontario Research Fund - Research Infrastructure (ORI-RI; 34107), and McMaster University. We would also like to thank the Centre for Emerging Device Technologies and Dr Peter Mascher for access to the variable angle spectral ellipsometer, the Biointerfaces Institute for access to the OCA 20 goniometer, and Drs Michael A. Brook and Yang Chen helpful conversations regarding silicon modification.

References

1 H. Vaisocherová, *et al.*, Rapid and sensitive detection of multiple microRNAs in cell lysate by low-fouling surface plasmon resonance biosensor, *Biosens. Bioelectron.*, 2015, **70**, 226–231.
2 H. Vaisocherová-Lísalová, *et al.*, Low-fouling surface plasmon resonance biosensor for multi-step detection of foodborne bacterial pathogens in complex food samples, *Biosens. Bioelectron.*, 2016, **80**, 84–90.
3 J. Wang and N. Hui, Zwitterionic poly(carboxybetaine) functionalized conducting polymer polyaniline nanowires for the electrochemical detection of carcinoembryonic antigen in undiluted blood serum, *Bioelectrochemistry*, 2019, **125**, 90–96.
4 N. Liu, N. Hui, J. J. Davis and X. Luo, Low Fouling Protein Detection in Complex Biological Media Supported by a Designed Multifunctional Peptide, *ACS Sens.*, 2018, **3**, 1210–1216.
5 J. Baggerman, M. M. J. Smulders and H. Zuilhof, Romantic Surfaces: A Systematic Overview of Stable, Biospecific, and Antifouling Zwitterionic Surfaces, *Langmuir*, 2019, **35**, 1072–1084.
6 F. Sun, *et al.*, Hierarchical zwitterionic modification of a SERS substrate enables real-time drug monitoring in blood plasma, *Nat. Commun.*, 2016, **7**, 1–9.
7 K. L. Prime and G. M. Whitesides, Adsorption of Proteins onto Surfaces Containing End-Attached Oligo(ethylene oxide): A Model System Using Self-Assembled Monolayers, *J. Am. Chem. Soc.*, 1993, **115**, 10714–10721.
8 R. F. Brady, Properties which influence marine fouling resistance in polymers containing silicon and fluorine, *Prog. Org. Coating*, 1999, **35**, 31–35.
9 C. Huang, N. D. Brault, Y. Li, Q. Yu and S. Jiang, Controlled Hierarchical Architecture in Surface-initiated Zwitterionic Polymer Brushes with Structurally Regulated Functionalities, *Adv. Mater.*, 2012, 1834–1837.
10 A. J. Keefe and S. Jiang, Poly(zwitterionic)protein conjugates offer increased stability without sacrificing binding affinity or bioactivity, *Nat. Chem.*, 2012, **4**, 59–63.
11 L. Zhang and Y. Sun, Poly(carboxybetaine methacrylate)-grafted silica nanoparticle: A novel carrier for enzyme immobilization, *Biochem. Eng. J.*, 2018, **132**, 122–129.
12 J. O. Zoppe, *et al.,* Surface-Initiated Controlled Radical Polymerization: State-of-the-Art, Opportunities, and Challenges in Surface and Interface Engineering with Polymer Brushes, *Chem. Rev.*, 2017, 1105–1318.
13 L. Michalek, L. Barner and C. Barner-Kowollik, Polymer on Top: Current Limits and Future Perspectives of Quantitatively Evaluating Surface Grafting, *Adv. Mater.*, 2018, **30**, 1–18.
14 W. Norde and D. Gags, Interaction of bovine serum albumin and human blood plasma with PEO-tethered surfaces: Influence of PEO chain length, grafting density, and temperature, *Langmuir*, 2004, **20**, 4162–4167.
15 C. J. Huang, Y. Li and S. Jiang, Zwitterionic polymer-based platform with two-layer architecture for ultra low fouling and high protein loading, *Anal. Chem.*, 2012, **84**, 3440–3445.
16 N. D. Brault, *et al.*, Two-layer architecture using atom transfer radical polymerization for enhanced sensing and detection in complex media, *Biomacromolecules*, 2012, **13**, 4049–4056.
17 Z. Cao, Q. Yu, H. Xue, G. Cheng and S. Jiang, Nanoparticles for drug delivery prepared from amphiphilic PLGA zwitterionic block copolymers with sharp contrast in polarity between two blocks, *Angew. Chem., Int. Ed.*, 2010, **49**, 3771–3776.
18 Y. Ma, *et al.*, Immobilization of poly(acrylamide) brushes onto poly(caprolactone) surface by combining ATRP and 'click' chemistry: Synthesis, characterization and

evaluation of protein adhesion, *Appl. Surf. Sci.*, 2015, **329**, 223–233.

19 H. Ju, B. D. McCloskey, A. C. Sagle, V. A. Kusuma and B. D. Freeman, Preparation and characterization of crosslinked poly(ethylene glycol) diacrylate hydrogels as fouling-resistant membrane coating materials, *J. Membr. Sci.*, 2009, **330**, 180–188.

20 D. Dong, *et al.*, *In Situ* 'clickable' Zwitterionic Starch-Based Hydrogel for 3D Cell Encapsulation, *ACS Appl. Mater. Interfaces*, 2016, **8**, 4442–4455.

21 Thermo Scientific, Pierce BCA Protein Assay Kit, 1296.9, *Pierce Biotechnol.*, 2011, **0747**, 1–7.

22 D. Ayediran, T. Bamkole, J. Hirst and I. Onyido, Kinetics of the Reactions of Piperidine, n-Butylamine, Morpholine, and Benzylamine with 2,4-Dinitrophenyl Phenyl Ether, *Tetrahedron*, 1974, 1970–1975.

23 D. B. Thomas, A. J. Convertine, R. D. Hester, A. B. Lowe and C. L. Mccormick, Hydrolytic Susceptibility of Dithioester Chain Transfer Agents and Implications in Aqueous RAFT Polymerizations, *Macromolecules*, 2004, 1735–1741.

24 C. L. McCormick and A. B. Lowe, Aqueous RAFT polymerization: Recent developments in synthesis of functional water-soluble (Co)polymers with controlled structures, *Acc. Chem. Res.*, 2004, **37**, 312–325.

25 B. Cao, L. Li, Q. Tang and G. Cheng, The impact of structure on elasticity, switchability, stability and functionality of an all-in-one carboxybetaine elastomer, *Biomaterials*, 2013, **34**, 7592–7600.

26 H. H. Kyaw, S. H. Al-Harthi, A. Sellai and J. Dutta, Self-organization of gold nanoparticles on silanated surfaces, *Beilstein J. Nanotechnol.*, 2015, **6**, 2345–2353.

27 N. Gurbuz, S. Demirci, S. Yavuz and T. Caykara, Synthesis of Cationic N-[3-(Dimethylamino)propyl]methacrylamide Brushes on Silicon Wafer via Surface-Initiated RAFT Polymerization, *J. Polym. Sci., Part A: Polym. Chem.*, 2011, **49**, 423–431.

28 M. Wang, *et al.*, Grafting of carboxybetaine brush onto cellulose membranes *via* surface-initiated ARGET-ATRP for improving blood compatibility, *Colloids Surf., B*, 2013, **103**, 52–58.

29 N. Aldred, G. Li, Y. Gao, A. S. Clare and S. Jiang, Modulation of barnacle (Balanus amphitrite Darwin) cyprid settlement behavior by sulfobetaine and carboxybetaine methacrylate polymer coatings, *Biofouling*, 2010, **26**, 673–683.

30 H. Ma, *et al.*, Surface initiated polymerization from substrates of low initiator density and its applications in biosensors, *ACS Appl. Mater. Interfaces*, 2010, **2**, 3223–3230.

31 N. D. Brault, *et al.*, Dry film refractive index as an important parameter for ultra-low fouling surface coatings, *Biomacromolecules*, 2012, **13**, 589–593.

32 N. D. Brault, *et al.*, Ultra-low fouling and functionalizable zwitterionic coatings grafted onto SiO2via a biomimetic adhesive group for sensing and detection in complex media, *Biosens. Bioelectron.*, 2010, **25**, 2276–2282.

33 W. Yang, H. Xue, W. Li, J. Zhang and S. Jiang, Pursuing 'zero' protein adsorption of poly(carboxybetaine) from undiluted blood serum and plasma, *Langmuir*, 2009, **25**, 11911–11916.

34 T. Riedel, *et al.*, Analytical Methods deposited on surface-grafted polymer brushes, *Anal. Methods*, 2016, 6415–6419.

35 Z. Zhang, T. Chao, S. Chen and S. Jiang, Superlow fouling sulfobetaine and carboxybetaine polymers on glass slides, *Langmuir*, 2006, **22**, 10072–10077.

36 X. Lin, *et al.*, Zwitterionic carboxybetaine polymers extend the shelf-life of human platelets, *Acta Biomater.*, 2020, 51–60.

37 B. Y. K. Chong, T. P. T. Le, G. Moad, E. Rizzardo and S. H. Thang, More versatile route to block copolymers and other polymers of complex architecture by living radical polymerization: the RAFT process, *Macromolecules*, 1999, **32**, 2071–2074.

38 J. Raula, *et al.*, Synthesis of gold nanoparticles grafted with a thermoresponsive polymer by surface-induced reversible-addition–fragmentation chain-transfer polymerization, *Langmuir*, 2003, **19**, 3499–3504.

39 P. S. Hegde, V. Karanikas and S. Evers, The Where, the When and the How of Immune Monitoring for Cancer Immunotherapies, *Clin. Cancer Res.*, 2016, 1865–1875.

40 J. B. Mcalvin, *et al.*, Antibody-modified conduits for highly selective cytokine elimination from blood Find the latest version: Antibody-modified conduits for highly selective cytokine elimination from blood, *JCI Insight*, 2018, **3**, e121133.

41 N. Y. Kostina, *et al.*, Antifouling Microparticles To Scavenge Lipopolysaccharide from Human Blood Plasma, *Biomacromolecules*, 2019, 959–968.

42 L. Di Lullo, *et al.*, Pathophysiology of the cardio-renal syndromes types 1–5: An uptodate, *Indian Heart J.*, 2017, **69**, 255–265.

43 C. Monard, T. Rimmelé and C. Ronco, Extracorporeal blood purification therapies for sepsis, *Blood Purif.*, 2019, **47**, 2–15.

